PCCP

Accepted Manuscript

This is an *Accepted Manuscript*, which has been through the Royal Society of Chemistry peer review process and has been accepted for publication.

Accepted Manuscripts are published online shortly after acceptance, before technical editing, formatting and proof reading. Using this free service, authors can make their results available to the community, in citable form, before we publish the edited article. We will replace this *Accepted Manuscript* with the edited and formatted *Advance Article* as soon as it is available.

You can find more information about *Accepted Manuscripts* in the Information for Authors.

Please note that technical editing may introduce minor changes to the text and/or graphics, which may alter content. The journal's standard Terms & Conditions and the Ethical guidelines still apply. In no event shall the Royal Society of Chemistry be held responsible for any errors or omissions in this *Accepted Manuscript* or any consequences arising from the use of any information it contains.

ROYAL SOCIETY OF CHEMISTRY

www.rsc.org/pccp

Charge Retention of Soft-Landed Phosphotungstate Keggin Anions on Self-Assembled Monolayers

AUTHORS

K. Don D. Gunaratne, Venkateshkumar Prabhakaran, Amity Andersen, Grant E. Johnson and Julia Laskin[*]

AUTHOR ADDRESS: Pacific Northwest National Laboratory, Physical Sciences Division, P.O. Box 999, MSIN K8-88, Richland, Washington 99352

[*]Author for correspondence: Julia.Laskin@pnnl.gov

KEYWORDS: Keggin polyoxometalates, ion soft landing, infrared reflection absorption spectroscopy, self-assembled monolayer surfaces, charge reduction, density functional theory.

Physical Chemistry Chemical Physics Accepted Manuscript

ABSTRACT

Soft landing of mass-selected ions onto surfaces often results in partial loss of charge that may affect the structure and reactivity of deposited species. In this study, Keggin phosphotungstate anions in two selected charge states, $PW_{12}O_{40}^{3-}$ ($WPOM^{3-}$) and $PW_{12}O_{40}^{2-}$ ($WPOM^{2-}$), were soft-landed onto different self-assembled monolayer (SAM) surfaces and examined using *in situ* infrared reflection absorption spectroscopy (IRRAS) and density functional theory (DFT) calculations. Partial retention of the 3- charge was observed when $WPOM^{3-}$ was soft-landed onto the fluorinated SAM (FSAM), while the charge state distribution was dominated by the 2- charge after both $WPOM^{3-}$ and $WPOM^{2-}$ were deposited onto a hydrophilic alkylthiol SAM terminated with cationic NH_3^+ functional groups (NH_3^+SAM). We found that during the course of the soft landing of $WPOM^{3-}$, the relative abundance of $WPOM^{3-}$ on FSAM decreased while that of $WPOM^{2-}$ increased. We propose that the higher stability of immobilized $WPOM^{2-}$ in comparison with $WPOM^{3-}$ makes it the preferred charge state of WPOM on both the FSAM and NH_3^+SAM. We also observe weaker binding of WPOM anions to SAMs in comparison with phosphomolybdate ions (MoPOM) reported previously (*J. Phys. Chem. C* **2014**, *118*, 27611–27622). The weaker binding of WPOM to SAMs is attributed to the lower reactivity of WPOM reported in the literature. This study demonstrates that both the charge retention and the reactivity of deposited anionic POM clusters on surfaces are determined by the type of addenda metal atoms in the cluster.

Physical Chemistry Chemical Physics Accepted Manuscript

Introduction

The effect of charge state on the structure and reactivity of complex molecules and clusters on surfaces has been described in numerous studies.[1-6] Soft landing of mass- and charge-selected ions provides a unique opportunity to examine the properties of the ion, the surface, and the influence of coverage on the final charge state distribution of a broad range of polyatomic ions deposited on surfaces.[7-14] Since the initial demonstration of charge retention of soft-landed ions by Cooks and co-workers,[15] this phenomenon has attracted considerable attention.[16-24] Understanding charge retention by soft-landed ions is important for controlling their chemical reactivity and electronic properties on surfaces. Our previous investigations used self-assembled monolayers of thiols on gold substrates (SAMs) as well-characterized thin insulating layers that are readily tailored for a particular application by varying the terminal functional group.[17-19, 21, 23-24] The charge retention of soft-landed ions has been mostly studied on hydrophobic alkylthiol SAMs (HSAM), their fluorinated analogs (FSAM), and hydrophilic SAMs terminated with carboxyl acid (COOH-SAM) or amine (NH_2-SAM, NH_3^+SAM) functional groups. The loss of the ionizing proton is the major charge reduction pathway for soft-landed protonated molecules such as proteins and peptides.[17-18, 22, 25] Retention of up to two ionizing protons and complete neutralization of protonated molecules was observed on FSAM and COOH-SAM surfaces, respectively, while HSAMs showed intermediate charge retention properties.[17-19] On the other hand, charge retention by native cations such as organometallics and small ligated metal clusters was observed to decrease in the order FSAM>COOH-SAM>HSAM.[21, 23, 26] Electron transfer through SAMs controlled by interface dipoles and the accumulation of ions on the surface was found to play a key role in charge reduction by soft-landed native cations.

In contrast to native cations, native anions such as polyoxometalates (POM) more readily retain their negative charge on SAMs.[24] POM and particularly Keggin anions are popular metal oxide building blocks for functional nanoscale systems[27-30] due to their outstanding stability[31] and diverse optical,[32] redox,[33] photochromic,[34] and catalytic properties.[35] The charge state of supported Keggin anions may affect these properties, which provides motivation for studying their charge retention. Previously, we demonstrated that soft-landing of molybdenum-based Keggin $[PMo_{12}O_{40}]^{n-}$ anions in the n = 2- and 3- charge states ($MoPOM^{2-}$ and $MoPOM^{3-}$) resulted in a similar charge distribution on both FSAM and HSAM surfaces.[24] We proposed that the barrier associated with electron detachment from the anion plays an important role in

Physical Chemistry Chemical Physics Accepted Manuscript

determining their charge retention on surfaces. This is different to the situation with native cations where charge reduction occurs by electron transfer through the SAM layer from the metal surface underneath.

In this study, we investigate charge retention by soft-landed $[PW_{12}O_{40}]^{n-}$ anions in the n = 2- and 3- charge states ($WPOM^{3-}$ and $WPOM^{2-}$) using *in situ* infrared reflection absorption spectroscopy (IRRAS) and density functional theory (DFT) calculations. The electronic properties of $WPOM^{3-}$ have been extensively investigated both experimentally and theoretically.[31, 36-40] It has been demonstrated that $MoPOM^{3-}$ is more reactive than $WPOM^{3-}$ both in solution and in the gas phase. For example, MoPOM undergoes dissociation at lower internal energies than WPOM in the gas phase.[41] Deshlara and Iglesia reported a combined experimental and theoretical study of the oxidative dehydrogenation of methanol on Keggin POM clusters.[42] Higher turnover frequencies were observed for POM clusters with Mo addenda atoms in comparison with POM clusters with W addenda atoms. Furthermore, higher absorption edge energies reflecting higher energy gaps between the highest occupied molecular orbital and lowest unoccupied molecular orbital (HOMO-LUMO gap) were observed in the UV/vis spectra of POM clusters with W addenda atoms. Because HOMO energies for all the Keggin anions examined in that study are similar,[42] the increase in the HOMO-LUMO gap reflects higher LUMO energies in POM clusters with W addenda atoms. These observations provide support for the higher reactivity of MoPOM toward gaseous reagents in comparison with WPOM.

Similarly, MoPOM is more reactive in aqueous media[33, 43] and is more readily protonated in solution than WPOM.[44-46] MoPOM is also more active than WPOM toward the oxidative dehydrogenation of methanol.[42] Hydrogen addition reaction may be described as a reaction involving the addition of an electron to an empty d-orbital of a metal atom accompanied by proton transfer to an O-atom. The higher efficiency of MoPOM toward hydrogen addition reaction in comparison with WPOM was attributed to the lower LUMO level in MoPOM, which facilitates electron transfer to MoPOM. Furthermore, MoPOM undergoes reversible electrochemical redox activity more readily than WPOM,[47] which is attributed to the lower HOMO-LUMO gap of MoPOM (2 eV) in comparison with WPOM (2.8 eV).[36] The vertical electron detachment energy of gas-phase MoPOM (1.94 eV) is lower than the value of 2.30 eV reported for WPOM[48] suggesting that charge retention by WPOM should be more efficient than MoPOM on the same SAM surfaces. Our results indicate better charge retention by $WPOM^{3-}$ in

Physical Chemistry Chemical Physics Accepted Manuscript

the initial stages of ion deposition followed by gradual loss of one electron over time resulting in formation of the exceptionally stable $WPOM^{2-}$ anion. In addition, we demonstrate much weaker binding of WPOM anions to SAMs in comparison with MoPOM anions. These findings have important implications for the immobilization of POMs on surfaces for applications in catalysis and electrochemical energy storage.

Experimental

Ion Soft-Landing

Sodium phosphotungstate hydrate ($Na_3[PW_{12}O_{40}].xH_2O$ CAS: 312696-30-3), methanol, 1H,1H,2H,2H-perfluorodecanethiol (FSAM), and 11-amino-1-undecanethiol hydrochloride (NH_2SAM) were purchased from Sigma-Aldrich (St. Louis, MO) and used as received. The WPOM solution for ion soft-landing experiments was prepared by first creating a 1 mM stock solution of sodium phosphotungstate hydrate in methanol and subsequently diluting it in methanol to a final concentration of ~100 μM.

SAM surfaces were prepared on 10 x 10 mm polycrystalline gold on silicon wafer surfaces (50 Å Ti adhesion layer, 1000 Å Au layer) purchased from Platypus Technologies (Madison, WI) following literature procedures.[49-51] As received gold substrates were sonicated in methanol for 10 minutes, dried using N_2 gas, cleaned in an ultraviolet/ozone cleaner (Model 135500, Boekel Industries Inc., Feasterville, PA) for 20 minutes, and immersed in a 1 mM solution of thiol in ethanol for ~24 hours. The substrates were then removed from the thiol solution, rinsed, and sonicated in methanol (FSAM) or 10% v/v acetic acid in ethanol (NH_3^+SAM) for 30 seconds to remove any loosely bound secondary thiol molecules and ensure protonation of the terminal amine groups. Finally, the substrates were rinsed with methanol, dried under nitrogen, and introduced into a deposition chamber for ion soft-landing experiments.

Soft-landing experiments were conducted using an ion deposition apparatus coupled with *in situ* IRRAS described in detail previously.[52-53] In this instrument, ions are produced using electrospray ionization[54] (ESI) and introduced into the vacuum system through a heated stainless steel capillary maintained at 120°C. Desolvated ions are subsequently transferred through an electrodynamic ion funnel[55] and radially focused in an rf only collisional quadrupole maintained at a pressure of 2 x 10^{-2} Torr by collisions with the background gas. Similar to MoPOM, ESI of

Physical Chemistry Chemical Physics Accepted Manuscript

WPOM predominately generates triply ($WPOM^{3-}$) and doubly charged species ($WPOM^{2-}$). A resolving quadrupole mass filter, (Extrel, Pittsburgh, PA) maintained at 8 x 10^{-5} Torr during ion deposition was used to select either $WPOM^{3-}$ or $WPOM^{2-}$ for deposition. Ions exiting the resolving quadrupole were focused using a series of three einzel lenses to produce a circular deposition area of ~3 mm in diameter on a SAM surface. The ion current on the surface was measured with a picoammeter (Model 9103, RBD Instruments, Bend, OR) throughout the deposition. In this study, the collision energy with the surface was in a range of 30-35 eV/charge and typical mass-selected ion currents were ~900 pA and ~400 pA for $WPOM^{3-}$ or $WPOM^{2-}$, respectively.

In-situ Infrared Reflection-Absorption Spectroscopy

In situ IRRAS experiments were performed using a Bruker Vertex 70 FTIR spectrometer (Bruker Optics, Billerica, MA) as described in detail in our previous publications.[52-53] During these experiments, IRRAS spectra are obtained during and after ion deposition by directing the IR beam exiting the spectrometer to the SAM surface through a ZnSe viewport mounted onto the deposition chamber. The IR beam passes through a mid-infrared ZnSe wire grid polarizer to produce *p*-polarized light and is focused on the surface using a gold-coated parabolic mirror with a focal length of 400 mm; the incident angle of the beam is 80º with respect to surface normal. The reflected light exiting the deposition chamber through a second ZnSe viewport is focused using two additional parabolic mirrors and detected using an externally mounted liquid nitrogen cooled mercury-cadmium-telluride (MCT) detector. The IR beam path is constantly purged with N_2 gas during the experiments to minimize atmospheric contributions to the signal. IR spectra were obtained by acquiring 1500 scans (~6 minutes) at 4 cm^{-1} resolution in 10 minutes intervals during the deposition.

Theoretical Methods

Hybrid DFT calculations were performed for the geometry optimization of the $WPOM^{3-}$, $WPOM^{2-}$, $WPOM^{1-}$, and $WPOM^{0}$ systems and for the calculation of the harmonic vibrational frequencies of these species. All calculations employed the B3LYP hybrid exchange-correlation functional. For the main group O and P atoms, the 6-311G* atomic basis set[56-57] was used, and, for the transition metal W atoms, the Stuttgart scalar relativistic effective core potential (ECP)

Physical Chemistry Chemical Physics Accepted Manuscript

and atomic basis set were employed.[58-60] The NWChem quantum chemistry code[61] was used to perform all geometry optimizations and harmonic frequency calculations.

Physical Chemistry Chemical Physics Accepted Manuscript

RESULTS AND DISCUSSION

In this study, we examined charge retention of multiply charged $[PW_{12}O_{40}]^{n-}$ anions (n=2, 3) soft-landed on FSAM and NH_3^+SAM surfaces. The FSAM surface was selected as a relatively inert hydrophobic substrate known to have a high barrier for electron transfer, resulting in charge retention of supported cations and anions.[15, 18, 21] In contrast, the NH_3^+SAM surface was selected as a positively charged hydrophilic substrate that has been shown previously to strongly bind soft-landed MoPOM anions through an electrostatic interaction.[24, 62] As discussed in our previous study,[24] charge reduction by POM anions on the FSAM surface involves electron detachment from the anion. For $WPOM^{3-}$, this results in formation of $[PW_{12}O_{40}]^{n-}$ species (n=0, 1, 2) referred to as $WPOM^0$, $WPOM^-$, and $WPOM^{2-}$, respectively. In comparison, both proton transfer and electron detachment may occur on the NH_3^+SAM surface. As mentioned earlier, the vertical electron detachment energy of 2.3 eV was determined experimentally for gas-phase $WPOM^{3-}$ ions.[48] Previously, we have demonstrated that electron detachment may be promoted by the kinetic energy of the ion at the time of collision with the surface which was held at ~90 eV in this study.[24] Alternatively, the electric field generated across the insulating SAM layer following deposition of anions may promote electron detachment from anions. Assuming complete charge retention, we estimate that approximately -6 V potential may build up across the 1 nm thick SAM following deposition of 2×10^{13} $WPOM^{3-}$ anions onto a 10 mm diameter spot. This potential is not high enough to block the incoming 90 eV ion beam but may be sufficiently large to induce electron detachment from $WPOM^{3-}$. In addition, this negative potential at the SAM-vacuum interface prevents electrons from tunneling through the SAM layer to the deposited species, which together with the Coulomb barrier present at each negatively charged cluster prevents the reverse process of electron attachment to the deposited negative species.

The IRRAS spectra obtained by soft landing ~2×10^{13} $WPOM^{3-}$ and $WPOM^{2-}$ anions on FSAM and NH_3^+SAM surfaces are presented in Figure 1; the relative intensities and positions of the major bands are summarized Table 1. Previously published IRRAS spectra of mass-selected $MoPOM^{3-}$ anions soft-landed on FSAM and NH_3^+SAM surfaces[24] are also shown in Figure 1 for comparison. Bridgeman reported a detailed analysis of the vibrational frequencies of isolated $WPOM^{3-}$ and related Keggin anions in the gas phase using DFT.[63-64] α-Keggin anions were found to have 22 active IR bands consistent with T_d symmetry.[64] By comparison with the

Physical Chemistry Chemical Physics Accepted Manuscript

experimental IR spectra,[65-66] Bridgeman assigned the major vibrational bands as follows. Two bands at 1066 and 969 cm^{-1} correspond to the asymmetric and symmetric combinations of the coupled P-O and W=O_t motions, respectively. The strong band at 981 cm^{-1} corresponds to the W=O_t stretching vibration while two bands at 915 and 840 cm^{-1} correspond to the W-O_{b2}-W and W-O_{b1}-W stretching motions of the two types of bridging oxygen atoms, respectively. Aside from the symmetric coupling band at 969 cm^{-1}, all other vibrational bands of the $WPOM^{3-}$ anion are shifted toward higher wavenumber in comparison with the $MoPOM^{3-}$ anion.[64] This shift in vibrational frequencies is attributed to the overall weaker bonds in $MoPOM^{3-}$ in comparison with $WPOM^{3-}$.[3-36, 64]

As shown in Figure 1 and Table 1, the major vibrational bands of the soft-landed $WPOM^{3-/2-}$ anions are observed at 1083, 990, 900, and 835 cm^{-1}. The asymmetric P-O/W=O_t combination band is labeled as P-O in Figure 1 while the symmetric P-O/W=O_t combination band (not labeled) is observed as a low wavenumber shoulder of the M=O_t band. Slight shifts in band positions are observed in the spectra of $WPOM^{3-}$ and $WPOM^{2-}$ anions on FSAM. These shifts and changes in peak shapes of $WPOM^{3-}$ and $WPOM^{2-}$ anions on FSAM will be discussed later. Meanwhile, almost identical IRRAS spectra were obtained for both charge states of WPOM on NH_3^+SAM. In fact, the IRRAS spectra of $WPOM^{3-}$ and $WPOM^{2-}$ anions soft-landed on NH_3^+SAM are very similar to the spectrum of $WPOM^{2-}$ on FSAM. In contrast, remarkably different IRRAS spectra dominated by broad features shifted toward lower wavenumbers in comparison with FSAM were reported previously for MoPOM anions soft-landed on NH_3^+SAM.[24] Furthermore, the shape of the Mo=O_t vibrational band of MoPOM on NH_3^+SAM showed a clear dependence on the initial charge state (3- vs. 2-) of the soft-landed anion, which is not the case for WPOM. The shifts in the position of the vibrational bands of MoPOM on NH_3^+SAM were attributed to the strong electrostatic attraction of the MoPOM anions and the positively charged terminal NH_3^+ groups on the surface while the broadening of the bands was attributed to the proton transfer from the terminal NH_3^+ group to the soft-landed anion.[24]

In agreement with previous experimental and theoretical studies,[63, 65] all the vibrational bands of the soft-landed WPOM are shifted toward higher wavenumbers in comparison with MoPOM. However, the experimentally observed shifts are substantially larger than the shifts predicted by electronic structure calculations of isolated POM clusters.[63] In addition, the WPOM

Physical Chemistry Chemical Physics Accepted Manuscript

bands are narrower than the MoPOM bands. Collectively, these observations may be attributed to the stronger bonds in WPOM[36, 64] and weaker interactions of this more stable cluster anion with SAM surfaces. The weak binding of WPOM to the positively charged NH_3^+SAM surface is further supported by the observation that soft-landed $WPOM^{3-}$ was easily washed away from this surface when immersed in 0.5 M H_2SO_4 electrolyte solution, which precluded its electrochemical characterization using cyclic voltammetry (CV). In contrast, CV of MoPOM on NH_3^+SAM examined in our previous study showed pronounced redox peaks that were stable for many cycles in the same electrolyte indicating strong immobilization of the MoPOM on the surface.[24] Because the proton affinity of MoPOM is higher than that of WPOM,[67] MoPOM is expected to form stronger hydrogen bonds with amino groups on the SAM surface than WPOM. Because proton affinities of both bridging and terminal O-atoms vary considerably with O-atom location,[42] multiple structures of proton-bound MoPOM are likely present on NH_3^+SAM. This heterogeneity in the MoPOM population contributes to the broadening of the infrared bands on NH_3^+SAM observed in our experiments.

To better understand the experimentally observed differences between IRRAS spectra of $WPOM^{3-}$ and $WPOM^{2-}$ anions on FSAM, we performed electronic structure calculations and vibrational frequency analysis of isolated $WPOM^{3-}$, $WPOM^{2-}$, $WPOM^-$ and neutral WPOM molecules. Calculated lowest-energy structures of the four charge states are shown in Figure 2; calculated vibrational frequencies of the major absorption bands are listed in Table 2 and the corresponding simulated infrared absorption spectra are shown in Figure 3. Experimental[65] and calculated[64] vibrational frequencies of $WPOM^{3-}$ and calculated vibrational frequencies of the different charge states on MoPOM[24] reported in previous studies are shown for comparison. A complete list of calculated absorption bands in the 1200-750 cm^{-1} range is given in Table S1 of the electronic supplementary information. Although the charge state has only a minor effect on the structure of WPOM (Figure 2), it has a pronounced influence on the vibrational frequencies of the major infrared bands (Figure 3 and Table 2). Similar to the charge state dependence of the vibrational features of MoPOM discussed in our previous study,[24] we observe a pronounced blue shift in the position of the $W{=}O_t$ band with a decrease in the charge state of WPOM. Furthermore, the separation between the $W{=}O_t$ and the symmetric P-O/$W{=}O_t$ combination band increases with a decrease in the charge state, and these bands are observed as two well-separated

Physical Chemistry Chemical Physics Accepted Manuscript

peaks in the simulated spectra of $WPOM^-$ and neutral WPOM. In contrast, the position of the asymmetric P-O/W=O_t combination band does not change with the WPOM charge state.

The position of the relatively weak W-O_{b2}-W bridging oxygen band shows a slight shift when the charge state decreases from 3- to 2- but the band separates into several low-abundance peaks with a further decrease in the charge state. Finally, the strong W-O_{b1}-W bridging oxygen band shows a substantial blue shift when the charge state decreases from 3- to 2- followed by a red shift for $WPOM^-$ and a slight blue shift for neutral WPOM. For $WPOM^{3-}$, the calculated W-O_{b1}-W and W-O_{b2}-W modes at 818 and 888 cm^{-1}, respectively, are observed as single peaks and the modes involving W=O_t coupling with both W-O_{b1}-W and W-O_{b2}-W are virtually IR silent. In contrast, band splitting is observed for $WPOM^{2-}$, $WPOM^{1-}$, and $WPOM^0$ in the W-O_{b1}-W (790-840 cm^{-1}) and W-O_{b2}-W (880 – 920 cm^{-1}) regions. For $WPOM^{2-}$, the band splitting is not as apparent as for the lower charge states. Nevertheless, two distinct bands at 818 and 822 cm^{-1} are observed for $WPOM^{2-}$ in the W-O_{b1}-W region and three bands at 886, 890, and 898 cm^{-1} are present in the W-O_{b2}-W region (Table 2). In contrast, the W-O_{b2}-W region of the calculated $WPOM^{1-}$ and $WPOM^0$ spectra contains a number of low-intensity bands. Band splitting observed in the W-O_{b1}-W and W-O_{b2}-W regions originates from the coupling between W-O_{b1}-W and W-O_{b2}-W vibrations with other modes. This coupling leads to a complex set of vibrational features in the corresponding frequency ranges with the upper range having a partial coupling of W=O_t motion along with the W-O_{b1}-W and W-O_{b2}-W mixed modes.

DFT calculations indicate that the position and the shape of the W=O_t band can be used as indicators of the charge state of soft-landed WPOM while the W-O_{b1}-W band can be used to distinguish between the 3- and 2- charge states of WPOM. We note that the absolute positions of the calculated vibrational bands are affected by the basis set used in DFT calculations while the relative trends in the charge state dependence of the calculated WPOM infrared spectra are robust. Furthermore, the positions of the experimental vibrational bands are affected by the strength of ion-surface interactions and surface selection rules. In the following discussion, we focus on comparison of peak shapes and qualitative trends in peak positions rather than the absolute position of the individual bands.

Physical Chemistry Chemical Physics Accepted Manuscript

It is reasonable to assume that a distribution of WPOM charge states on the SAM surface is generated by soft-landing of $WPOM^{3-}$ or $WPOM^{2-}$ anions. Our previous studies demonstrated that instantaneous charge loss occurs during ion-surface collision followed by a slower charge reduction by thermalized ions trapped on the insulating SAMs.[21, 25] To further understand the charge distribution of the soft-landed WPOM, we combined the calculated spectra of the four charge states in different proportions to simulate the experimental infrared signature of a distribution of the WPOM charge states on FSAM. The results of this simulation are compared with the experimental spectra of the soft-landed $WPOM^{3-}$ and $WPOM^{2-}$ in Figure 4. The best qualitative agreement between the experimental and simulated spectra of the soft-landed $WPOM^{3-}$ was obtained by combining 25% $WPOM^{3-}$, 60% $WPOM^{2-}$, and 15% $WPOM^{1-}$ while the experimental spectrum of the soft-landed $WPOM^{2-}$ was well-reproduced by combining 80% $WPOM^{2-}$ and 20% $WPOM^{1-}$. In these simulations, particular attention was given to the shape of the $W{=}O_t$ band and the position of the $W\text{-}O_{b1}\text{-}W$ bridging oxygen band.

Both the experimental and simulated spectra show little or no change in the position and shape of the asymmetric $P\text{-}O/W{=}O_t$ combination band and the $W\text{-}O_{b2}\text{-}W$ bridging oxygen band. The simulation also reproduces the blue shift in the position of the $W\text{-}O_{b1}\text{-}W$ bridging oxygen band in the experimental spectrum of the soft-landed $WPOM^{2-}$. Finally, the shape of the $W{=}O_t$ band is qualitatively reproduced using the two distributions of the WPOM charge states. Despite the qualitative nature of such a comparison, it clearly indicates that a relatively small but measurable fraction of the soft-landed $WPOM^{3-}$ retain their charge state while a larger fraction is converted into $WPOM^{2-}$ on FSAM. In contrast, $WPOM^{2-}$ is more robust and better retains its initial charge state when soft-landed onto FSAM. Based on these simulations, we propose that the lower wavenumber shoulder of the $W{=}O_t$ band of the soft-landed $WPOM^{3-}$ corresponds to the remaining intact $WPOM^{3-}$ anions while the higher wavenumber feature corresponds to $WPOM^{2-}$. The close correspondence between the experimental IRRAS spectra of $WPOM^{3-}$ and $WPOM^{2-}$ anions soft-landed on NH_3^+SAM and $WPOM^{2-}$ on FSAM suggests that NH_3^+SAM predominately retains the 2- charge state of WPOM. Proton transfer from the charged terminal groups of NH_3^+SAM to POM anions is a likely charge reduction mechanism on this surface.[24] However, because protonation of POM has only a small effect on the position of the infrared

Physical Chemistry Chemical Physics Accepted Manuscript

bands,[24] it is difficult to distinguish between charge reduction by protonation and by electron detachment on NH_3^+SAM based on IRRAS data.

Our previous study showed that the intensities of the major bands of MoPOM soft-landed on FSAM increase steadily during the course of the deposition and their shapes remain largely unchanged.[24] This observation indicates that rapid charge loss during ion deposition is the major mechanism of charge reduction for MoPOM on FSAM. In contrast, in this study we observed substantial change in the shapes of the W-O_{b1}-W and W=O_t bands over time during soft-landing of $WPOM^{3-}$ and no change in the shapes of these bands during deposition of $WPOM^{2-}$ as shown in Figure 5. Specifically, early in the deposition process both the W-O_{b1}-W and W=O_t bands of the soft-landed $WPOM^{3-}$ show pronounced features at lower wavenumbers that most likely correspond to the intact $WPOM^{3-}$. The relative abundance of these features in comparison with the higher wavenumber features within the same vibrational bands gradually decreases as the soft-landing deposition progresses. In contrast, very similar peak shapes are observed for all WPOM bands during soft-landing of $WPOM^{2-}$. These results can be rationalized assuming slow charge reduction by the soft-landed $WPOM^{3-}$ on FSAM that does not occur when $WPOM^{2-}$ is soft-landed on this surface. These observations are consistent with the relatively small fraction of intact $WPOM^{3-}$ and a substantial abundance of the $WPOM^{2-}$ retained on FSAM after soft-landing of $WPOM^{3-}$. Furthermore, this experiment supports the exceptional stability of $WPOM^{2-}$ on FSAM inferred from other experimental observations discussed earlier. Our results demonstrate substantial differences in charge retention by MoPOM and WPOM and identify $WPOM^{2-}$ as an exceptionally stable charge state of WPOM on SAM surfaces.

CONCLUSIONS

Interaction of POM anions with surfaces may affect their charge state, redox properties, and reactivity. In this study, we examined charge retention by soft landed $WPOM^{3-}$ and $WPOM^{2-}$ anions on SAM surfaces using *in situ* IRRAS experiments and DFT calculations. We demonstrate substantial differences in charge retention and interaction of MoPOM and WPOM with the same SAM surfaces. Specifically, we observe weaker binding of WPOM anions to SAM surfaces. The difference in the binding energy of WPOM and MoPOM to SAMs is reflected in substantially narrower IRRAS bands of soft-landed WPOM shifted toward higher wavenumbers in comparison with broader peaks for MoPOM. Furthermore, the weaker binding of WPOM to

Physical Chemistry Chemical Physics Accepted Manuscript

the positively charged NH_3^+SAM surface resulted in efficient removal of the deposited WPOM by the electrolyte solution and precluded its electrochemical characterization. These results indicate that MoPOM forms strong bonds with the NH_3^+SAM surface, which is consistent with the lower LUMO energy of MoPOM in comparison with WPOM. Similarly we can deduce that higher electronic stability of WPOM anion is most likely responsible for the observed weaker binding of these species to SAMs. Our results indicate that ion-surface interactions and charge retention of deposited ions plays an important role in determining the stability and reactivity of immobilized ions. It follows that stable immobilization of MoPOM on amine-terminated surfaces may be used for the fabrication of stable functionalized electrode surfaces or catalytically active substrates. In contrast, WPOM is less susceptible to stable immobilization through adsorption.

Comparison of the positions and shapes of the major vibrational bands of WPOM obtained from IRRAS experiments with the results of DFT calculations indicates efficient charge retention of $WPOM^{2-}$ on both FSAM and NH_3^+SAM. Meanwhile a relatively small fraction of $WPOM^{3-}$ is retained on FSAM and the relative abundance of this charge state gradually decreases over time during ion deposition. In contrast, charge reduction by MoPOM occurs on a much shorter timescale, which is consistent with the lower electron binding energy of MoPOM in comparison with WPOM. This work indicates that the charge retention and structural stability are important factors which determine the reactivity of soft landed ions on surfaces. Furthermore, it also presents a pathway to manipulate stable reactive surfaces for catalysis and electrochemical energy storage applications.

ACKNOWLEDGEMENTS

This work was supported by the U.S. Department of Energy (DOE), Office of Science, Office of Basic Energy Sciences, Chemical Sciences, Geosciences & Biosciences Division. The research was performed using EMSL, a national scientific user facility sponsored by the DOE's Office of Biological and Environmental Research and located at Pacific Northwest National Laboratory (PNNL). PNNL is operated by Battelle for DOE under Contract DE-AC05-76RL01830.

ELECTRONIC SUPPLEMENTARY INFORMATION (ESI).

Calculated vibrational frequencies of $WPOM^{3-}$, $WPOM^{2-}$, $WPOM^{1-}$, and $WPOM^{0}$ in the 1200-800 cm^{-1} range.

Physical Chemistry Chemical Physics Accepted Manuscript

REFERENCES

1. Yoon, B.; Häkkinen, H.; Landman, U.; Wörz, A. S.; Antonietti, J.-M.; Abbet, S.; Judai, K.; Heiz, U., *Science* **2005,** *307*, 403-407.
2. Swart, I.; Sonnleitner, T.; Repp, J., *Nano Lett.* **2011,** *11*, 1580-1584.
3. Fu, Y.-S.; Zhang, T.; Ji, S.-H.; Chen, X.; Ma, X.-C.; Jia, J.-F.; Xue, Q.-K., *Phys. Rev. Lett.* **2009,** *103*, 257202.
4. Sterrer, M.; Risse, T.; Martinez Pozzoni, U.; Giordano, L.; Heyde, M.; Rust, H.-P.; Pacchioni, G.; Freund, H.-J., *Phys. Rev. Lett.* **2007,** *98*, 096107.
5. Leoni, T.; Guillermet, O.; Walch, H.; Langlais, V.; Scheuermann, A.; Bonvoisin, J.; Gauthier, S., *Phys. Rev. Lett.* **2011,** *106*, 216103.
6. Repp, J.; Meyer, G.; Olsson, F. E.; Persson, M., *Science* **2004,** *305*, 493-495.
7. Cooks, R. G.; Ast, T.; Pradeep, T.; Wysocki, V., *Accounts of Chemical Research* **1994,** *27*, 316-323.
8. Grill, V.; Shen, J.; Evans, C.; Cooks, R. G., *Rev. Sci. Instrum.* **2001,** *72*, 3149-3179.
9. Gologan, B.; Green, J. R.; Alvarez, J.; Laskin, J.; Cooks, R. G., *Phys Chem Chem Phys* **2005,** *7*, 1490-1500.
10. Laskin, J.; Wang, P.; Hadjar, O., *Phys. Chem. Chem. Phys.* **2008,** *10*, 1079-1090.
11. Johnson, G. E.; Hu, Q. C.; Laskin, J., *Annual Review of Analytical Chemistry* **2011,** *4*, 83-104.
12. Cyriac, J.; Pradeep, T.; Kang, H.; Souda, R.; Cooks, R. G., *Chem. Rev.* **2012,** *112*, 5356-5411.
13. Verbeck, G.; Hoffmann, W.; Walton, B., *Analyst* **2012,** *137*, 4393-4407.
14. Johnson, G. E.; Gunaratne, D.; Laskin, J., *Mass Spectrom. Rev.* **2015**, n/a-n/a.
15. Miller, S. A.; Luo, H.; Pachuta, S. J.; Cooks, R. G., *Science* **1997,** *275*, 1447-1450.
16. Shen, J. W.; Yim, Y. H.; Feng, B. B.; Grill, V.; Evans, C.; Cooks, R. G., *Int. J. Mass Spectrom.* **1999,** *183*, 423-435.
17. Hadjar, O.; Futrell, J. H.; Laskin, J., *J. Phys. Chem. C* **2007,** *111*, 18220-18225.
18. Laskin, J.; Wang, P.; Hadjar, O.; Futrell, J. H.; Alvarez, J.; Cooks, R. G., *Int. J. Mass Spectrom.* **2007,** *265*, 237-243.
19. Hadjar, O.; Wang, P.; Futrell, J. H.; Laskin, J., *J. Am. Soc. Mass Spectrom.* **2009,** *20*, 901-906.
20. Laskin, J.; Wang, P.; Hadjar, O., *J. Phys. Chem. C* **2009,** *114*, 5305-5311.
21. Johnson, G. E.; Priest, T.; Laskin, J., *ACS Nano* **2011,** *6*, 573-582.
22. Peng, W.-P.; Johnson, G. E.; Fortmeyer, I. C.; Wang, P.; Hadjar, O.; Cooks, R. G.; Laskin, J., *Phys. Chem. Chem. Phys.* **2011,** *13*, 267-275.
23. Johnson, G. E.; Priest, T.; Laskin, J., *J. Phys. Chem. C* **2012,** *116*, 24977-24986.
24. Gunaratne, K. D. D.; Johnson, G. E.; Andersen, A.; Du, D.; Zhang, W.; Prabhakaran, V.; Lin, Y.; Laskin, J., *J. Phys. Chem. C* **2014,** *118*, 27611-27622.
25. Alvarez, J.; Futrell, J. H.; Laskin, J., *J. Phys. Chem. A* **2005,** *110*, 1678-1687.
26. Johnson, G. E.; Wang, C.; Priest, T.; Laskin, J., *Anal. Chem.* **2011,** *83*, 8069-8072.
27. Katsoulis, D. E., *Chem. Rev.* **1998,** *98*, 359-388.
28. Song, Y.-F.; Tsunashima, R., *Chem. Soc. Rev.* **2012,** *41*, 7384-7402.
29. Miras, H. N.; Yan, J.; Long, D.-L.; Cronin, L., *Chem. Soc. Rev.* **2012,** *41*, 7403-7430.
30. Long, D.-L.; Tsunashima, R.; Cronin, L., *Angew. Chem. Int. Ed.* **2010,** *49*, 1736-1758.
31. Lopez, X.; Carbo, J. J.; Bo, C.; Poblet, J. M., *Chem. Soc. Rev.* **2012,** *41*, 7537-7571.
32. Suzuki, K.; Tang, F.; Kikukawa, Y.; Yamaguchi, K.; Mizuno, N., *Angew. Chem.* **2014,** *126*, 5460-5464.
33. Sadakane, M.; Steckhan, E., *Chem. Rev.* **1998,** *98*, 219-238.
34. Yamase, T., *Chem. Rev.* **1998,** *98*, 307-326.
35. Long, D. L.; Tsunashima, R.; Cronin, L., *Angewandte Chemie-International Edition* **2010,** *49*, 1736-1758.
36. López, X.; Maestre, J. M.; Bo, C.; Poblet, J.-M., *J. Am. Chem. Soc.* **2001,** *123*, 9571-9576.
37. Guo, Y.-R.; Pan, Q.-J.; Wei, Y.-D.; Li, Z.-H.; Li, X., *J. Mol. Struct.* **2004,** *676*, 55-64.

Physical Chemistry Chemical Physics Accepted Manuscript

38. Wen, S.; Guan, W.; Wang, J.; Lang, Z.; Yan, L.; Su, Z., *Dalton Trans.* **2012,** *41*, 4602-4607.
39. Uehara, K.; Miyachi, T.; Nakajima, T.; Mizuno, N., *Inorg. Chem.* **2014,** *53*, 3907-3918.
40. Waters, T.; Huang, X.; Wang, X.-B.; Woo, H.-K.; O'Hair, R. A. J.; Wedd, A. G.; Wang, L.-S., *J. Phys. Chem. A* **2006,** *110*, 10737-10741.
41. Gunaratne, K. D.; Prabhakaran, V.; Johnson, G.; Laskin, J., *J. Am. Soc. Mass Spectrom.* **2015,** *26*, 1027-1035.
42. Deshlahra, P.; Iglesia, E., *J. Phys. Chem. C* **2014,** *118*, 26115-26129.
43. Papaconstantinou, E.; Pope, M. T., *Inorg. Chem.* **1967,** *6*, 1152-1155.
44. Barrows, J. N.; Pope, M. T., *Advances in Chemistry Series* **1990,** *226*, 403.
45. Keita, B.; Nadjo, L., *Journal of Electroanalytical Chemistry and Interfacial Electrochemistry* **1987,** *227*, 77-98.
46. Pope, M. T.; Varga, G. M., *Inorg. Chem.* **1966,** *5*, 1249-1254.
47. Zhang, J.; Bond, A. M.; MacFarlane, D. R.; Forsyth, S. A.; Pringle, J. M.; Mariotti, A. W. A.; Glowinski, A. F.; Wedd, A. G., *Inorg. Chem.* **2005,** *44*, 5123-5132.
48. Waters, T.; Huang, X.; Wang, X.-B.; Woo, H.-K.; O'Hair, R. A. J.; Wedd, A. G.; Wang, L.-S., *J. Phys. Chem. A* **2006,** *110*, 10737-10741.
49. Fukushima, H.; Seki, S.; Nishikawa, T.; Takiguchi, H.; Tamada, K.; Abe, K.; Colorado, R.; Graupe, M.; Shmakova, O. E.; Lee, T. R., *J. Phys. Chem. B* **2000,** *104*, 7417-7423.
50. Wallwork, M. L.; Smith, D. A.; Zhang, J.; Kirkham, J.; Robinson, C., *Langmuir* **2001,** *17*, 1126-1131.
51. Wang, H.; Chen, S.; Li, L.; Jiang, S., *Langmuir* **2005,** *21*, 2633-2636.
52. Hu, Q.; Wang, P.; Gassman, P. L.; Laskin, J., *Anal. Chem.* **2009,** *81*, 7302-7308.
53. Hu, Q.; Wang, P.; Laskin, J., *Phys. Chem. Chem. Phys.* **2010,** *12*, 12802-12810.
54. Fenn, J.; Mann, M.; Meng, C.; Wong, S.; Whitehouse, C., *Science* **1989,** *246*, 64-71.
55. Shaffer, S. A.; Prior, D. C.; Anderson, G. A.; Udseth, H. R.; Smith, R. D., *Anal. Chem.* **1998,** *70*, 4111-4119.
56. Krishnan, R.; Binkley, J. S.; Seeger, R.; Pople, J. A., *J. Chem. Phys.* **1980,** *72*, 650-654.
57. McLean, A. D.; Chandler, G. S., *J. Chem. Phys.* **1980,** *72*, 5639-5648.
58. Bergner, A.; Dolg, M.; Küchle, W.; Stoll, H.; Preuß, H., *Mol. Phys.* **1993,** *80*, 1431-1441.
59. Kaupp, M.; Schleyer, P. v. R.; Stoll, H.; Preuss, H., *J. Chem. Phys.* **1991,** *94*, 1360-1366.
60. Dolg, M.; Stoll, H.; Preuss, H.; Pitzer, R. M., *J. Phys. Chem.* **1993,** *97*, 5852-5859.
61. Valiev, M.; Bylaska, E. J.; Govind, N.; Kowalski, K.; Straatsma, T. P.; Van Dam, H. J. J.; Wang, D.; Nieplocha, J.; Apra, E.; Windus, T. L.; de Jong, W. A., *Comput. Phys. Commun.* **2010,** *181*, 1477-1489.
62. Wang, S.; Du, D., *Sens. Actuators, B* **2003,** *94*, 282-289.
63. Bridgeman, A. J., *Chem. Eur. J.* **2004,** *10*, 2935-2941.
64. Bridgeman, A. J., *Chemical Physics* **2003,** *287*, 55-69.
65. Rocchiccioli-Deltcheff, C.; Fournier, M.; Franck, R.; Thouvenot, R., *Inorg. Chem.* **1983,** *22*, 207-216.
66. Yurchenko, E. N.; Bugaev, V. I., *Journal of Molecular Structure* **1984,** *115*, 71-74.
67. Ganapathy, S.; Fournier, M.; Paul, J. F.; Delevoye, L.; Guelton, M.; Amoureux, J. P., *J. Am. Chem. Soc.* **2002,** *124*, 7821-7828.

Physical Chemistry Chemical Physics Accepted Manuscript

Table 1. Experimental vibrational frequencies (in cm^{-1}) and relative peak intensities of $WPOM^{3-}$ and $WPOM^{2-}$ soft landed onto FSAM and NH_3^+SAM surfaces.

WPOM-SAM		**P-O**	**W=O_t**	**W-O_{b2}-W**	**W-O_{b1}-W**
FSAM $WPOM^{3-}$	wavenumber	1084	991	901	833
	rel. intensity	*18*	*25*	*16*	*42*
NH_3^+SAM $WPOM^{3-}$	wavenumber	1082	989	899	833
	rel. intensity	*17*	*22*	*16*	*46*
FSAM $WPOM^{2-}$	wavenumber	1084	991	899	837
	rel. intensity	*22*	*22*	*13*	*43*
NH_3^+SAM $WPOM^{2-}$	wavenumber	1082	991	899	835
	rel. intensity	*18*	*21*	*17*	*44*

Physical Chemistry Chemical Physics Accepted Manuscript

Table 2. Calculated vibrational frequencies (in cm^{-1}) of isolated $WPOM^{3-}$, $WPOM^{2-}$, $WPOM^{1-}$, and $WPOM^{0}$ for the major bands in the 1200-750 cm^{-1} range. Previously reported calculated (calc) and experimental (exp) values for $WPOM^{3-}$ and different charge states of MoPOM are listed for comparison. Multiple maxima observed in composite bands are separated by a "/".

Mode	**$WPOM^{3-}$**			**$WPOM^{2-}$**	**$WPOM^{1-}$**	**$WPOM^{0}$**
	This study	*Calc. [64]*	*Exp. [65]*	*This study*	*This study*	*This study*
P-O, W=O_t asymmetric coupling	1058	1066	1080	1060	1052/1058/1066	1055/1058
W=O_t	974	981	976	994	1008	1022
P-O, W=O_t symmetric coupling	966	969		982	992/996	1004
W-O_{b2}-W	888	915	895	886/890/898	892/906/914	892/906/916
W-O_{b1}-W	818	840	810	822/828	798/818	820/826/838
	$MoPOM^{3-}$ [24]			**$MoPOM^{2-}$**[24]	**$MoPOM^{1-}$**[24]	**$MoPOM^{0}$**[24]
P-O	1055	1060	1063	1055	1064	1065
Mo=O_t	969	969	955	983	993	1001
Mo-O_{b2}-Mo	878	881	880	874	886	888
Mo-O_{b1}-Mo	819	815	805	817	841	797

Physical Chemistry Chemical Physics Accepted Manuscript

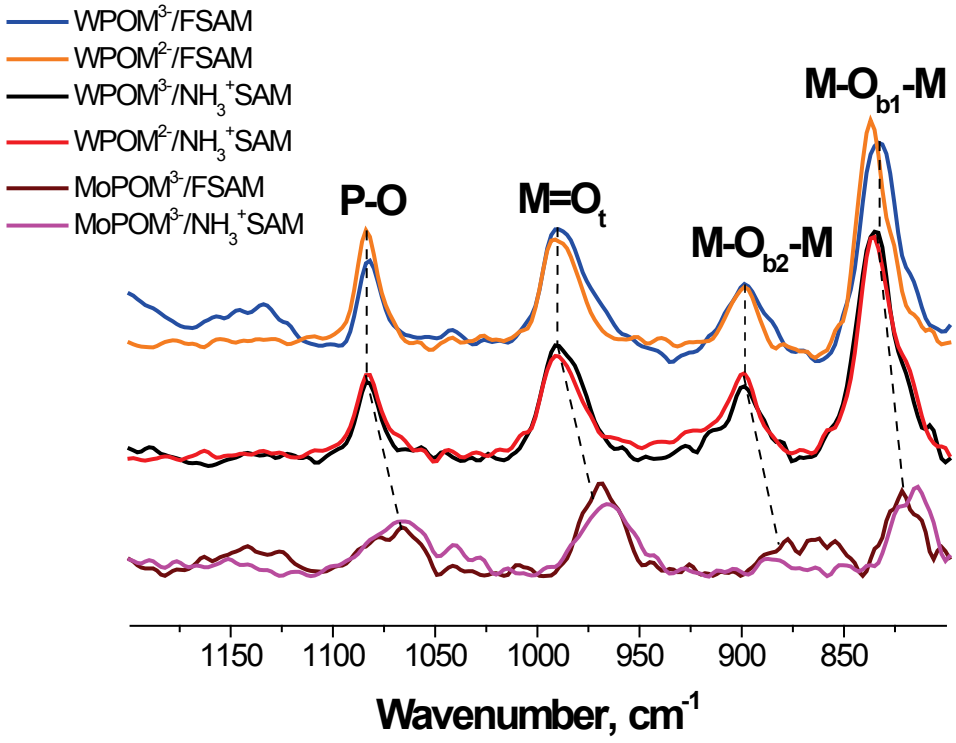

Figure 1. IRRAS spectra obtained by depositing ~2 x 10^{13} $WPOM^{3-}$ and $WPOM^{2-}$ ions on FSAM and NH_3^+SAM surfaces. IRRAS spectra of ~2 x 10^{13} $MoPOM^{3-}$ ions deposited on FSAM and NH_3^+SAM surfaces are shown for comparison. Peak positions and assignments are provided in Tables 1 and 2. The dashed lines highlight the key vibrational features of the POM.

Physical Chemistry Chemical Physics Accepted Manuscript

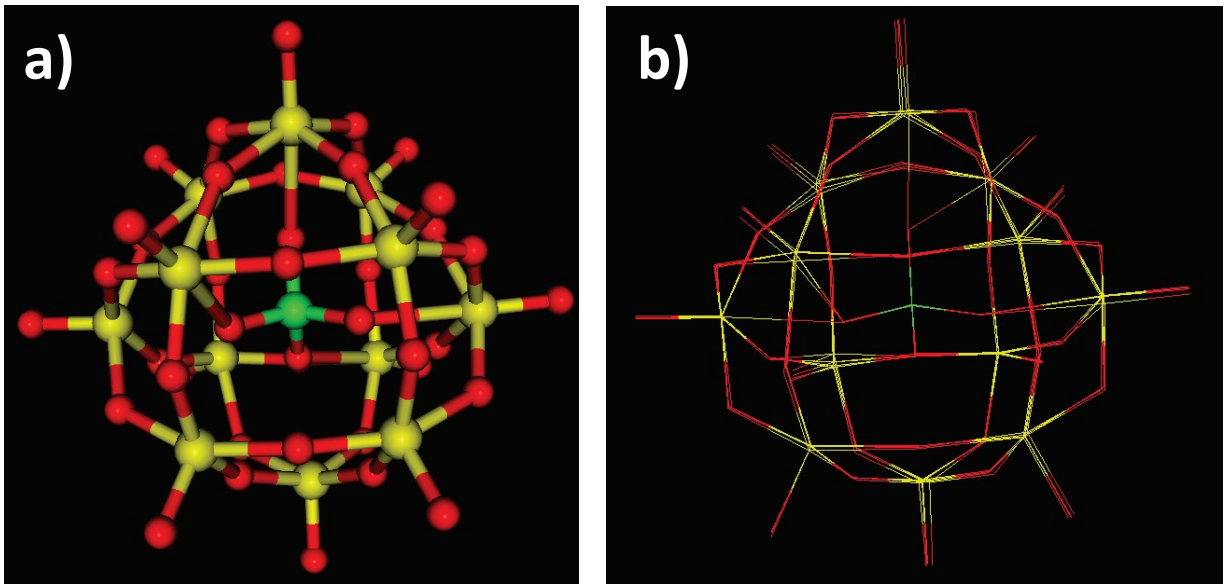

Figure 2. a) Calculated lowest energy structure of the triply charged Keggin phosphotungstate ($WPOM^{3-}$) in the gas phase; b) overlaid structures of the 3-, 2-, 1-, and 0 WPOM charge states examined in DFT calculations. Color coding: P - green, O - red, W - yellow.

Physical Chemistry Chemical Physics Accepted Manuscript

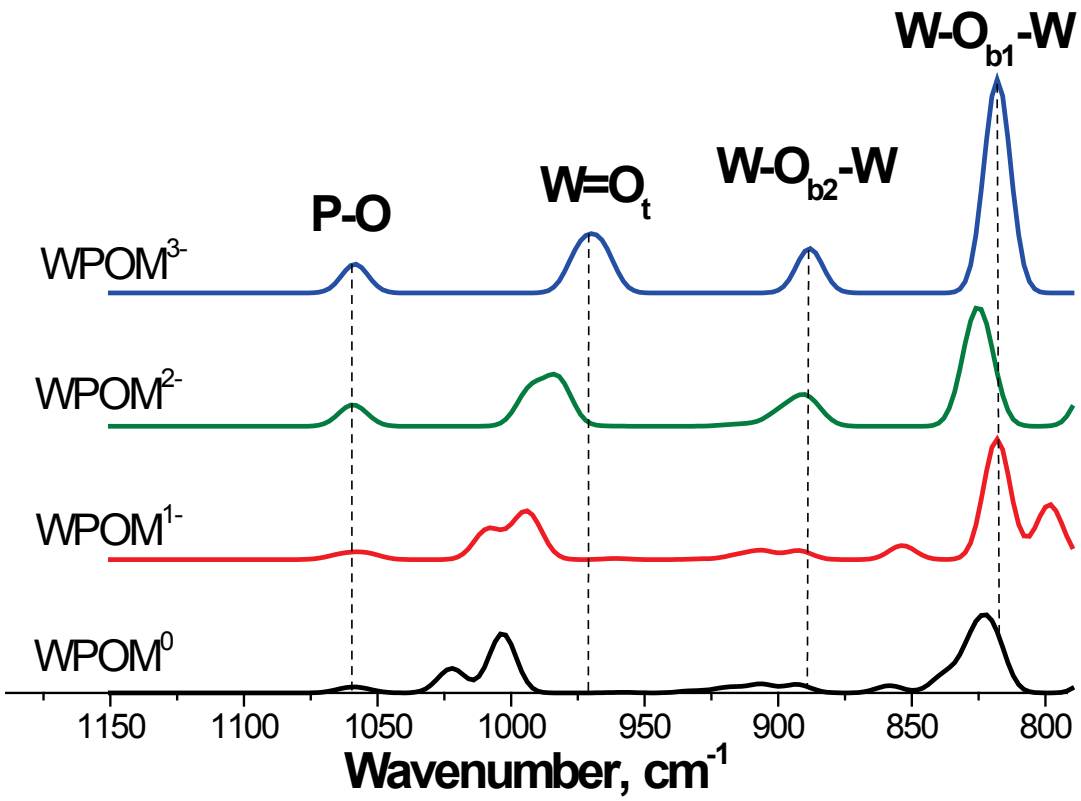

Figure 3. Simulated infrared absorbance spectra of isolated $WPOM^{3-}$ (blue), $WPOM^{2-}$ (green), $WPOM^{-}$ (red), and $WPOM^{0}$ (black) constructed using vibrational frequencies and intensities obtained from DFT calculations. The dashed lines highlight the major absorption bands of $WPOM^{3-}$ obtained from DFT calculations and illustrate their shifts with different charge states.

Physical Chemistry Chemical Physics Accepted Manuscript

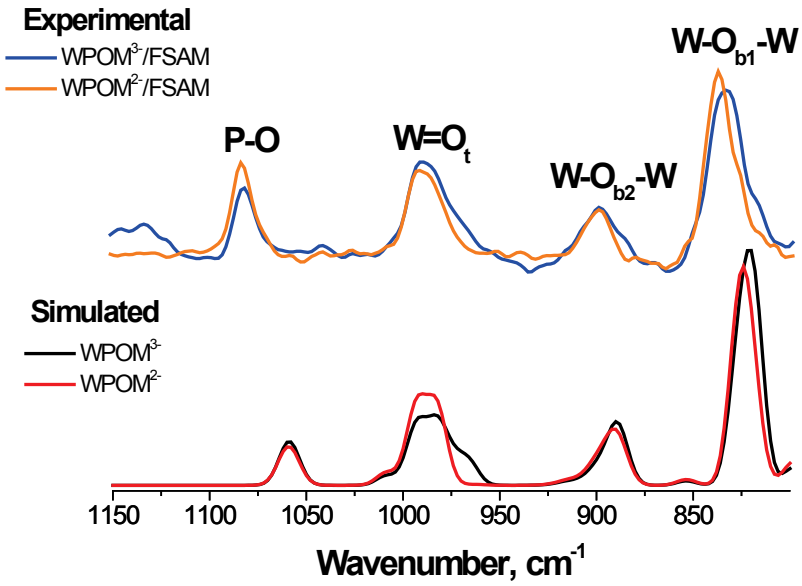

Figure 4. Experimental and simulated spectra of $WPOM^{3-}$ (blue and black traces) and $WPOM^{2-}$ (orange and red traces) deposited on FSAM. Simulated spectra were obtained by combining DFT calculated infrared spectra of different charge states of isolated WPOM in different proportions. The simulated spectrum of soft landed $WPOM^{3-}$ showing the best qualitative agreement with the experimental data was obtained by combining 25% $WPOM^{3-}$, 60% $WPOM^{2-}$, and 15% $WPOM^{1-}$; the simulated spectrum of $WPOM^{2-}$ showing the best qualitative agreement with the experimental data was obtained by combining 80% $WPOM^{2-}$ and 20% $WPOM^{1-}$.

Physical Chemistry Chemical Physics Accepted Manuscript

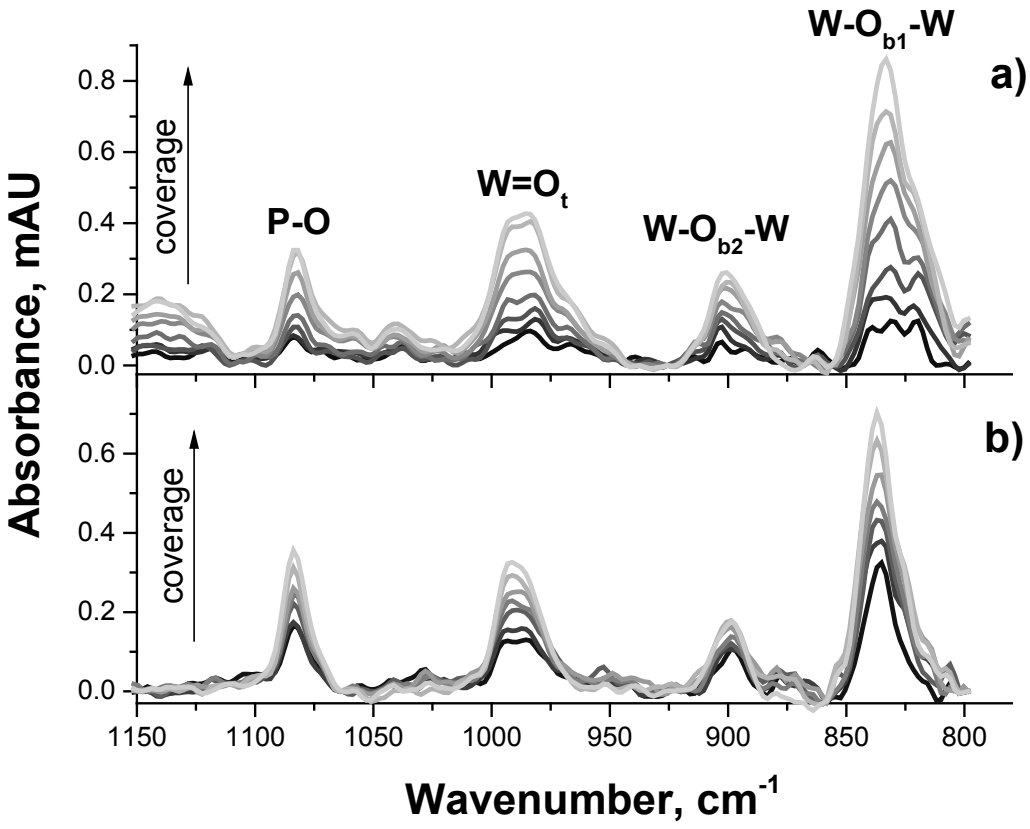

Figure 5. Time-dependent IRRAS spectra acquired at regular intervals during deposition of a) $WPOM^{3-}$ and b) $WPOM^{2-}$ ions on FSAM surface. The maximum coverage corresponds to ~2 x 10^{13} ions.

Physical Chemistry Chemical Physics Accepted Manuscript

TOC Graphic

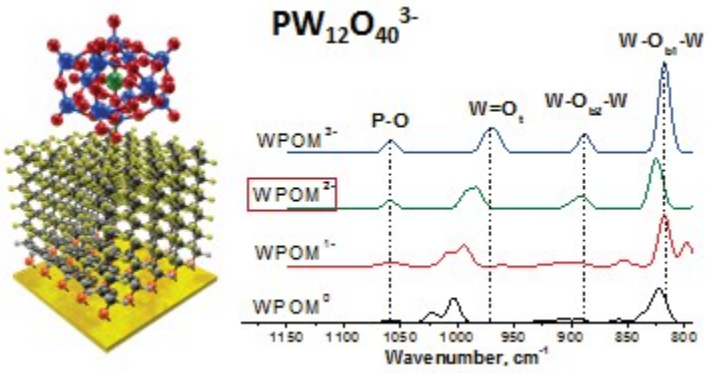

Preferential immobilization of the 2- charge state observed for polyoxotungstate Keggin anions soft-landed onto self-assembled monolayer surfaces.

Physical Chemistry Chemical Physics Accepted Manuscript